Available online at www.sciencedirect.com

ScienceDirect

Geochimica et Cosmochimica Acta 165 (2015) 389–406

Geochimica et Cosmochimica Acta

www.elsevier.com/locate/gca

The behavior of biologically important trace elements across the oxic/euxinic transition of meromictic Fayetteville Green Lake, New York, USA

Jeff R. Havig [a,*], Michael L. McCormick [b], Trinity L. Hamilton [c], Lee R. Kump [a]

[a] Dept. of Geosciences, PSU, University Park, PA 16803, USA
[b] Dept. of Biology, Hamilton College, Clinton, NY 13323, USA
[c] Dept. of Biological Sciences, University of Cincinnati, OH 45221, USA

Received 27 January 2015; accepted in revised form 18 June 2015; Available online 24 June 2015

Abstract

Trace elements are central components of enzymes that catalyze many of the essential reactions mediated by life. The redox sensitive nature of trace elements also permits their use as a record of ancient ocean conditions preserved in the geologic record. Trace element geochemistry in modern stratified systems is often used as a proxy for the redox state of the ancient oceans, which are thought to have been largely anoxic. In the present study, we examined trace element behavior of simultaneously collected samples at a heretofore unprecedented depth resolution (1–0.25 m intervals) throughout the redox-stratified water column of Fayetteville Green Lake, N.Y. (FGL), a 53 m deep meromictic lake under euxinic conditions similar to those thought to have been prevalent in Proterozoic oceans. Among characterized Proterozoic ocean analogs, FGL represents an understudied proxy in terms of trace elements, with characteristics of low salinity and high sulfate. In the FGL water column, spikes in the concentration of dissolved Mn, Fe and Co are coincident with the transition from oxic to euxinic conditions, and are associated with a decrease in dissolved Mo concentration. In contrast, the concentration of dissolved Ni did not vary across this transition despite the dramatic shift in redox state. From these data we present a one dimensional model for element transport and cycling through the water column to the sediments. Collectively, this comprehensive analysis of water column geochemistry provides insight into the effects of biogeochemical cycling in stratified systems on dissolved trace element concentrations in the water column. This study, in concert with characterization of other early Earth analogs, will greatly enhance the use of trace elements in interpreting the geologic record.

1. INTRODUCTION

Trace elements are central components of enzymes that catalyze many reactions mediated by and essential to life. Fe serves numerous functions in organisms including haem (a Fe^{2+}-containing cofactor) iron for O_2 transport, electron transfer, and protection from super-oxides. Mn and Mo also serve crucial roles—for instance, the former is present in the active site of photosystem II, and the latter a key component of the Mo-dependent nitrogenase enzyme which catalyzes dinitrogen reduction to ammonia. Furthermore, the redox sensitive nature of trace elements with elevated abundance in Earth's crust (e.g., Fe and Mn) can be exploited as couples for energy yielding metabolic reactions.

Trace elements may also record past redox conditions, and have been used to constrain the redox state of the oceans through earth history (e.g., Arnold et al., 2004;

* Corresponding author at: Dept. of Geology, University of Cincinnati, Cincinnati, OH 45221, USA. Tel.: +1 509 637 6375.
E-mail address: jeffhavig@gmail.com (J.R. Havig).

http://dx.doi.org/10.1016/j.gca.2015.06.024
0016-7037/

Rouxel et al., 2005; Scott et al., 2008; Planavsky et al., 2011; Poulton and Canfield, 2011; Reinhard et al., 2013). These studies, and many others, are bolstered by data gathered from modern aquatic stratified systems and have suggested that the earth's oceans were locally to globally stratified, with a potentially transient oxic surface over anoxic to euxinic deeper water (Kump et al., 2005; Meyer and Kump, 2008; Severmann et al., 2008; Planavsky et al., 2011; Poulton and Canfield, 2011), throughout the Proterozoic and even into the Archaean and Cenozoic, encompassing over half of Earth's history.

Reduction potential is the main factor controlling the solubility and speciation of many trace elements in aquatic systems, driven by the presence of oxygen or sulfide and influenced by the biogeochemical cycling of the endemic microbial community (Murray, 1987; Hamilton-Taylor and Davison, 1995). Trace element concentrations in stratified systems are also linked to the presence of oxygen and/or sulfide and microbial activity, with the transition between the upper oxic zone and lower euxinic zone demarking the greatest change in trace element composition. Stratified conditions in oceans on the early Earth have been implied as potential drivers of enzymatic evolution based on arguments that the availability of trace metals varies with redox conditions (Anbar and Knoll, 2002; Saito et al., 2003; Dupont et al., 2010).

Stratified aquatic systems ranging from fresh to hypersaline have been characterized with regard to trace element geochemistry (e.g. Paul Lake, MI, Taillefert and Gaillard, 2002; Lago di Cadagno, Switzerland, Tonolla et al., 1998 and Dahl et al., 2010; ice-covered Lake A, Canada, Gibson et al., 2002; Framvaren Fjord, Norway, Jacobs et al., 1985; Yao and Millero, 1995; Mariager Fjord, Denmark, Ramsing et al., 1996; Drammensfjord, Norway, Öztürk, 1995; the Black Sea, Lewis and Landing, 1991, 1992; Orca Basin, Gulf of Mexico, Van Cappellen et al., 1998). From this body of literature, we can predict general behaviors of trace elements in stratified systems, including lower dissolved Mn and Fe concentration and higher dissolved Mo concentration in the oxic zone, and higher dissolved Mn and Fe and lower dissolved Mo concentration in the euxinic zone. However, most of these studies are based on samples not collected from a single time point, requiring an assumption that samples collected across hours or even days are directly comparable. Furthermore, previous studies have focused on fresh water systems with low sulfate concentrations (e.g., Lago di Cadagno, <2 mM SO_4^{2-}) or saline to hypersaline marine water systems replete with sulfate in the water column (e.g., Framvaren Fjord, >10 mM SO_4^{2-}; Black Sea, ~18 mM SO_4^{2-}; Orca Basin, 33.5 mM SO_4^{2-}), but not on low salinity, high sulfate systems. In all modern aquatic stratified systems, biological sulfate reduction is the source of sulfide that maintains euxinia; therefore, in freshwater systems, sulfate availability is the main limiting factor for sulfide generation (Cappenberg, 1974; Lovley and Klug, 1983; Sinke et al., 1992; Lamers et al., 1998). Thus, stratified fresh water systems with high sulfate concentrations represent an important gap in our understanding of redox gradients and trace metal behavior. In order to produce a dataset that is devoid of temporal influences in water column geochemistry in a stratified freshwater system with intermediate levels of sulfate, we conducted the first simultaneous measurement of trace element concentrations coupled to water chemistry throughout the water column of Fayetteville Green Lake, N.Y.

Fayetteville Green Lake (FGL) near Fayetteville, N.Y. (Fig. 1) was the first meromictic lake to be described in North America (Eggleton, 1931), and the water column geochemistry has been studied for nearly 100 years (Eggleton, 1931, 1956; Deevey et al., 1963; Turano and Rand, 1967; Takahashi et al., 1968; Brunskill and Ludlam, 1969; Jelacic, 1970; Torgersen et al., 1981; Fry, 1986; Thompson et al., 1990; Zerkle et al., 2010; Hunter, 2012; Oduro et al., 2013). These studies indicate FGL has an oxic mixolimnion from 0 to 15 m depth that is supersaturated with dissolved O_2 (up to 420 μM), a more saline and euxinic monimolimnion (total sulfide concentration of up to 1.86 mM) from ~21 m to the bottom at 53 m, and a 6 m thick chemocline (boundary zone between the mixolimnion and the monimolimnion) from 15 to ~21 m that transitions between the oxic and euxinic layers, the bottom of which is demarked by a redoxcline and a dense population of anoxygenic photosynthetic bacteria (microbial plate) (Fig. 1). In contrast to previous studies of stratified systems, FGL is unique in that the water is fresh to slightly brackish with a sulfate concentration of 11.7 to 15.1 mM (Brunskill and Ludlam, 1969), which falls between the low sulfate fresh water and high sulfate saline to hypersaline water end members. The elevated sulfate concentration (compared to fresh water systems) results from input of groundwater flowing through gypsum-bearing shale. The sulfate concentration of FGL is also similar to the values estimated for Proterozoic oceans immediately following the Great Oxidation Event (Planavsky et al., 2012).

Previous measurements of Mn made at FGL indicated low concentrations in the mixolimnion, high concentrations in the monimolimnion and a peak in Mn concentration at the chemocline (Torgersen et al., 1981), while the concentrations of other trace metals have not been investigated. In the present study, we examined trace element behavior in the redox-stratified water column of FGL using a simultaneous high depth-resolution sampling apparatus (McCormick et al., 2014). We collected samples through the 53 m water column of FGL in November, 2012 and July, 2013 to determine concentrations of five biologically-important trace elements (Mn, Fe, Co, Ni, and Mo) coupled to contextual geochemical analyses at a higher depth resolution than has been reported to date for any stratified system. These data, coupled to bulk pore water values, suggest a complex interaction of biogeochemical cycling and transport of elements from the water column to the sediments. We propose a conceptual model that describes the cycling of Mn and Fe in the water column and transport of Mn, Fe, and Mo from the water column to the sediments.

2. METHODS

High depth-resolution sampling was conducted using the sampling apparatus described in McCormick et al.

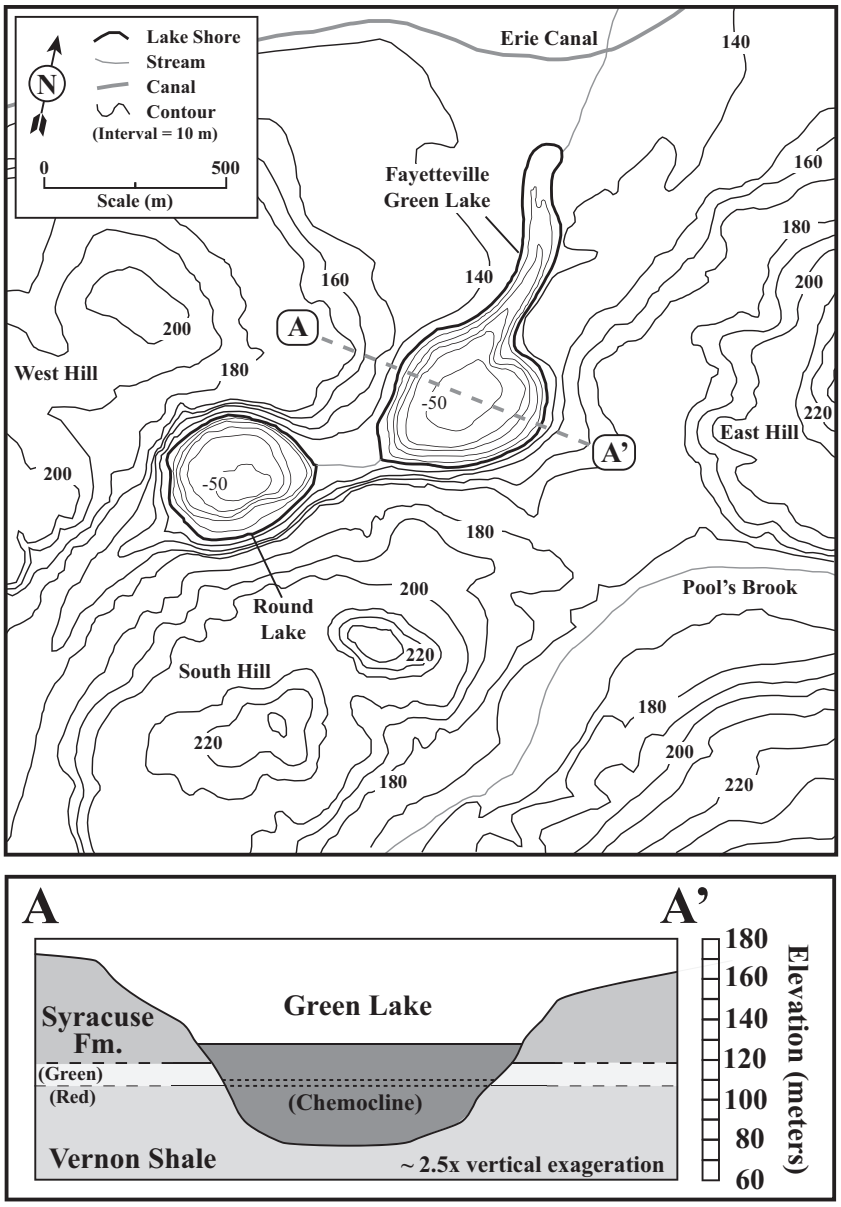

Fig. 1. Map and cross section of Fayetteville Green Lake, N.Y., modified from Hilfinger et al. (2001), Jelacic (1970), Takahashi et al. (1968), and Muller (1967). Letters and dashed grey lines denote cross section. Stratigraphy based on generalized stratigraphic column from Muller (1967).

(2014). In short, syringes were placed under vacuum with an affixed glass pipette tip, attached to a 52 m sampling device (every meter, except between 16 and 24 m, where syringes were deployed every 0.25 m), and were triggered simultaneously with a messenger. Following triggering, the syringes were retrieved, immediately placed on ice (~4 °C), and transported to Hamilton College, Clinton, NY where they were processed within ~6 h of collection. Depths lacking data are a result of syringe plunger failure due to high pressures at depth.

Sediment cores were collected to a depth of ~40 cm using 2 inch diameter gravity corers fitted with ~50 cm long polycarbonate liners. Upon retrieval, sediment cores were capped without headspace and kept on ice (~4 °C) until processed. For analysis, the top 30 cm of sediments were extruded and homogenized in a glove box with a 100% N_2 headspace. Pore water was recovered by centrifugation of sediments (50 mL at 3000 rpm and 4 °C for 10 min) and subsequently filtered and stored as described below.

Temperature, conductivity, pH, turbidity, and oxidation–reduction potential (ORP) were determined *in situ* with a calibrated YSI 6600 multi-parameter sonde probe (YSI Incorporated, Yellow Springs, OH, USA) on days that samples were collected. ORP was not collected for July, 2013. Total sulfide ($\Sigma S^{2-} = H_2S + HS^- + S^{2-}$) concentration was determined from 1 ml sample aliquots dispensed into 2 mL screw top microcentrifuge tubes pre-filled with 0.5 mL of 20% w/w zinc acetate solution.

Samples were then vortexed for 5 s and stored at 4 °C in the dark until analysis. Sulfide was determined colorimetrically using the method of Cline (1969).

Water samples (10 mL) were filtered through 25 mm diameter, 0.22 μm polyethersulfone syringe filters (VWR International, Radnor, PA) into 15 mL centrifuge tubes that had been pre-soaked in 18.2 MΩ/cm DI water. Anion samples from November, 2012 (for chloride and nitrate) were analyzed with a Dionex ICS2500 ion chromatography (IC) system (Dionex, Sunnyvale, CA, USA). Detection limits were 11 μM for chloride, and 6.5 μM for nitrate. Samples from November, 2012 for total ammonium were analyzed with a Hach DR2700 spectrophotometer on filtered water samples that had been left refrigerated and exposed to oxygenated atmosphere to eliminate potential sulfide interference. Samples were diluted with 18.2 MΩ/cm DI water and analyzed using Hach Method 8155 for determining total ammonia within the range of 0.01–0.50 mg/L (0.6–28 μM). November, 2012 cation samples were determined via a Thermo X-Series II Quadrupole collision cell technology enabled inductively-coupled plasma mass spectrometer (Thermo Fisher Scientific, Waltham, MA). Anions (Cl^-, SO_4^{2-}, and NO_3^-) and cations (Ca^{2+}, Mg^{2+}, Na^+, and NH_4^+) from July, 2013 were quantified by IC using parallel Metrohm 861 Advanced Compact IC units. Dissolved inorganic carbon (DIC) and dissolved organic carbon (DOC) analyses were conducted by the Stable Isotope Facility at University of California, Davis. DIC was analyzed using a GasBench II system interfaced to a Delta V Plus isotope ratio mass spectrometer (IR-MS) (Thermo Scientific, Bremen, Germany). DOC was determined via an O.I. Analytical Model 1030 TOC Analyzer (O.I. Analytical, College Station, TX) interfaced to a PDZ Europa 20-20 isotope ratio mass spectrometer (Sercon Ltd., Cheshire, UK) utilizing a GD-100 Gas Trap Interface (Graden Instruments) for concentration and isotope ratio determination. Trace element analysis was conducted via a Thermo X-Series II Quadrupole collision cell technology enabled inductively-coupled plasma mass spectrometer (Thermo Fisher Scientific, Waltham, MA). Single element certified standards (CPI International) and NIST Standard Reference Material 1643e were used for quantification of all trace elements analyzed.

Details of analytical procedures for determining major ions, dissolved carbon, and trace elements can be found in the Supplementary online material (SOM), as well as data tables for all results. Anion speciation and saturation indices calculations are also described in the SOM.

3. RESULTS

3.1. General geochemistry

Temperature profiles from November, 2012 and July, 2013 show the monimolimnion remained unchanged at ~7 °C while the mixolimnion showed considerable seasonal variation (Fig. 2). Relatively uniform profiles for temperature and pH (Fig. 2) as well as dissolved oxygen (D.O., Fig. 3) in the mixolimnion for November suggests recent mixing to a depth of at least 15 m (top of the chemocline). At both time points an 'elbow' in temperature is observed through the chemocline (the transition zone between the mixolimnion and the monimolimnion) and pH decreases from ~8 in the mixolimnion to 6.8 in the monimolimnion. Levels of total dissolved solids (TDS) were less (~2 g/L) above the chemocline and increase to ~2.8 g/L below the chemocline (Fig. 2). A peak in turbidity associated with a dense microbial community (microbial plate) was observed at the base of the chemocline (~20 m) in both the

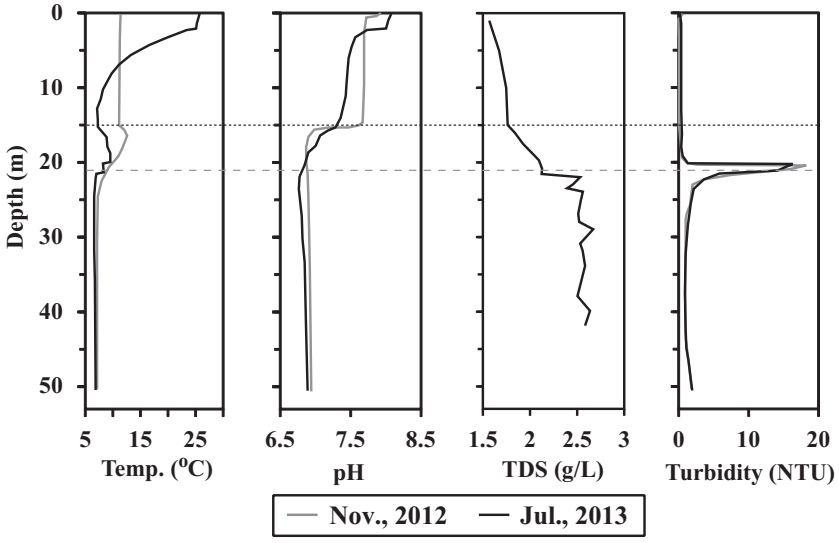

Fig. 2. Water temperature (Temp.), salinity, pH, and turbidity measured via SONDE cast plotted against water depth. Grey lines represent values from November 10, 2012, black lines from July 16, 2013. Temperature is reported in degrees Celsius (°C), total dissolved solids (TDS) as g/L, and turbidity in nephelometric turbidity units (NTU). Black dotted line indicates the top of the chemocline, and the grey dashed line the bottom of the chemocline.

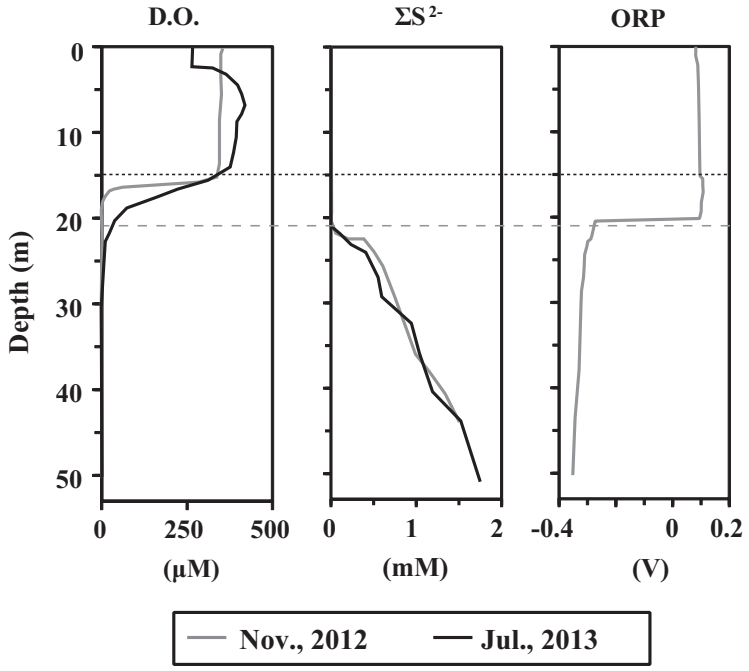

Fig. 3. Dissolved oxygen (D.O.), total sulfide (sum of H_2S and HS^-, reported as ΣS^{2-}), and oxidation/reduction potential (ORP) reported for Fayetteville Green Lake, N.Y., plotted against depth from surface. Grey lines represent values from November 10, 2012, black lines from July 16, 2013. Black dotted line indicates the top of the chemocline, and the grey dashed line the bottom of the chemocline.

November, 2012 and July, 2013 profiles (Fig. 2). D.O. concentration drops from super saturation at 15 m to below detection limits near 20 m in both November and July. In contrast, total dissolved sulfide (ΣS^{2-}) concentration increases to above detection limits (>10 μM) between 20.5 and 20.75 m. This transition is concurrent with an abrupt shift in oxidation reduction potential (ORP) from +91 mV to −274 mV at 20.3 m (Fig. 3).

The concentration of major cations and anions throughout the water column were similar regardless of sample collection time (Fig. 4). In general, concentrations were lower in the mixolimnion and higher in the monimolimnion with the exception of nitrate (Fig. 4). Mixolimnion average values were similar for November and July for Na^+ (1.1 and 1.0 mM), Mg^{2+} (2.5 and 2.3 mM), Ca^{2+} (10.5 and 10.9 mM), HCO_3^- (2.9 and 2.6 mM), and Cl^- (1.4 and 1.5 mM). Average SO_4^{2-} values were 9.9 mM in July (not determined for November). Monimolimnion average values were all greater than the mixolimnion, and were similar for November and July for Na^+ (1.3 and 1.4), Mg^{2+} (3.4 and 3.0 mM), Ca^{2+} (15.5 and 15.0 mM), HCO_3^- (3.6 and 3.9 mM), and Cl^- (2.0 and 2.1 mM). Average SO_4^{2-} values were 14.3 mM in July. The concentration of nitrate was ~60 μM in the mixolimnion but was not detectable below the chemocline (detection limit ~1 μM). Ammonium concentrations were of similar magnitude to those of nitrate in the chemocline, although increasing with depth and rising to over 500 μM in the monimolimnion.

3.2. Trace elements

The redox sensitive trace element concentrations show a complex behavior across the transition zone from the oxic mixolimnion to the euxinic monimolimnion (Fig. 5). Lower total dissolved Mn concentration was observed in the mixolimnion (average values of 16 and 15 nM for November and July, respectively). In contrast, the average dissolved Mn concentration was over three orders of magnitude higher in the monimolimnion (6.8 and 6.4 μM for November and July, respectively) and the highest concentrations were observed in the chemocline (61.4 μM at 21.25 m in November and 58.5 μM at 20.5 m in July) (Fig. 5). Dissolved Mn concentration exhibits a decrease with depth in the monimolimnion below the chemocline peak, dropping from ~10 μM at 25 m to below 5 μM at the greatest depths (Fig. 5). The oxic mixolimnion has lower dissolved Fe (average of 28 nM in November, 17 nM in July) due to the insolubility of Fe^{3+} oxy-hydroxides. In contrast, the euxinic monimolimnion below 24 m has an average dissolved Fe concentration that is higher (185 nM in November, 154 nM in July) (Fig. 5). There is a peak in dissolved Fe concentration associated with the chemocline, at 21.75 m (3.2 μM) in November and at 20.75 m (2.0 μM) in July, which is consistently 0.25–0.5 m below the peak in dissolved Mn, but within the turbidity peak and the euxinic zone. Dissolved Co follows the concentration pattern of dissolved Mn in both November, 2012 and July 2013, with lower concentration in the mixolimnion (average of 1.8 and 1.7 nM, respectively), peak concentrations that coincide with peak dissolved Mn concentration (86.2 nM at 21.25 m in November and 32.9 nM at 20.5 m in July), and elevated concentration in the monimolimnion that are roughly stable below 25 m (9.6 and 8.9 nM, respectively) (Fig. 5). The concentration of dissolved nickel did not show any deviation throughout the water column of FGL, with an

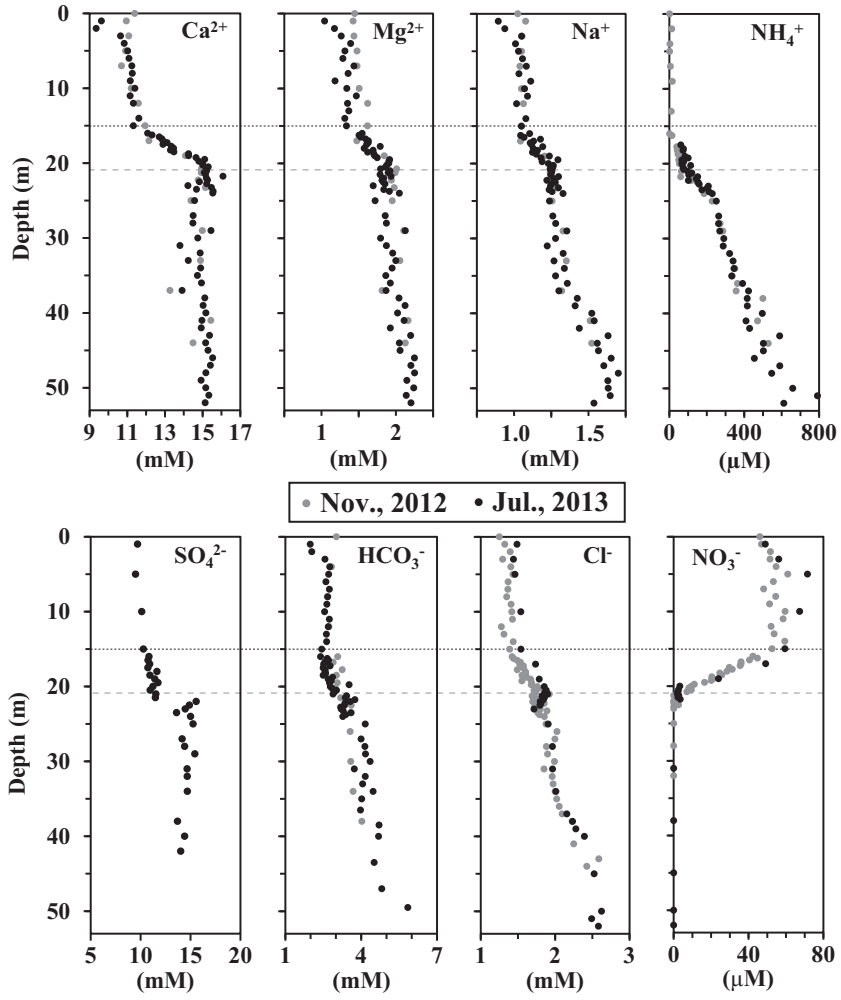

Fig. 4. Major cations (Ca^{2+}, Mg^{2+}, Na^{+}, and NH_4^{+}) and anions (SO_4^{2-}, HCO_3^{-}, Cl^{-}, and NO_3^{-}) reported for samples collected from Fayetteville Green Lake, N.Y. on November 10, 2012 and July 16, 2013, plotted against depth from surface. HCO_3^{-} values calculated from DIC concentrations (as described in Section 2). Black dotted line indicates the top of the chemocline, and the grey dashed line the bottom of the chemocline.

average value of ~91 nM (Fig. 5). The average concentration of dissolved Mo in the FGL mixolimnion was 186 and 179 nM, and 17 and 13 nM in the monimolimnion for November 2012 and July 2013, respectively, with the oxic zone dissolved Mo concentration higher than average ocean values (~105 nM, Collier, 1985).

4. DISCUSSION

4.1. Characterization of the water column

The water column at FGL consists of three zones, the upper mixolimnion from the surface to 15 m, characterized by D.O. at or above saturation, temperatures that change dramatically from fall to summer, and relatively high pH (Figs. 2 and 3); the chemocline from 15 to 21 m, which transitions from oxic at the top to euxinic at the bottom, and exhibits a temperature 'elbow'; and the lower monimolimnion from 21 to 53 m, characterized by sulfide concentrations greater than 50 μM, temperatures that are stable and consistent at ~7 °C, and pH values near 7. Elevated temperature of the surface water in July likely reflects seasonal warming and accumulation of runoff. The 'elbow' in temperature measured through the chemocline was observed at both time points. The peak of this elbow is higher in November than in July, despite the warmer surface temperature suggesting a lag in time for heat transfer and thermal cycling at this depth relative to the lake surface.

The turbidity peak located at the base of the chemocline and the top of the monimolimnion coincides with an abundance of photosynthetic microorganisms as is observed in other meromictic systems such as Mahoney Lake and Lago di Cadagno (Northcote and Hall, 1983; Overmann et al., 1991; Camacho et al., 2001). A study of pigment concentrations conducted from May through November of 2011 at FGL showed a strong correlation between the turbidity peak, redoxcline, and the occurrence of photosynthetic pigments (Hunter, 2012). That study also suggested a seasonal shift in the photosynthetic community composition and turbidity maximum from a purple sulfur bacteria (PSB) predominant plate (based on abundance of

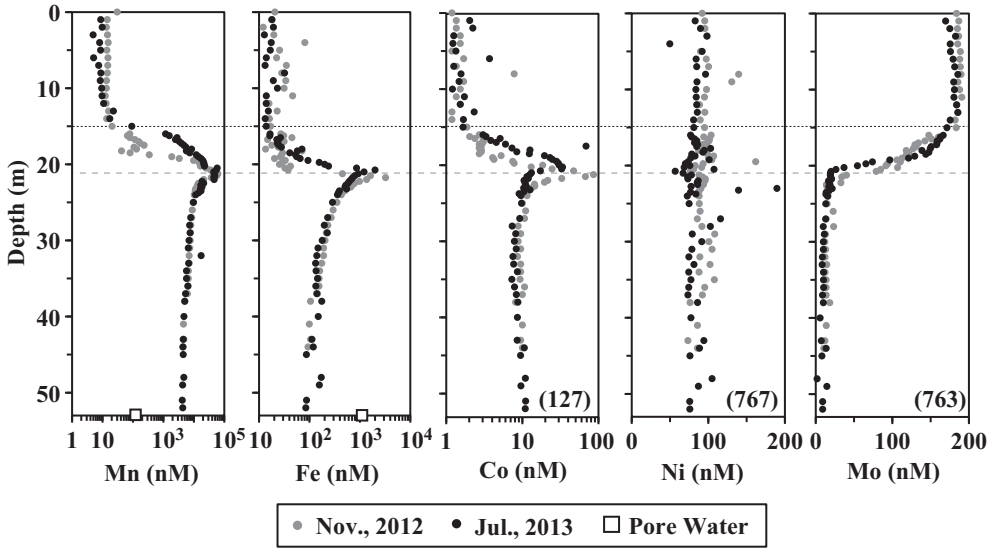

Fig. 5. Manganese, iron, cobalt, nickel and molybdenum concentration reported for Fayetteville Green Lake, N.Y., plotted against depth from surface. Solid grey circles represent values from November 10, 2012, solid black circles from July 16, 2013. Open squares are pore water values from bulk sediments collected November, 10, 2012, with off scale values given in parentheses. Black dotted line indicates the top of the chemocline (15 m), and grey dashed line the bottom of the chemocline (21 m). Note semi-log plots for Mn, Fe, and Co.

bacteriochlorophyll (BChl) *a*) at a depth of 20 m in May to a green sulfur bacteria (GSB) predominant plate (based on abundance of bacteriochlorophyll (BChl) *e*) at a depth of 21 m in September. The observation of different photosynthetic pigments with depth throughout the redoxcline is consistent with other stratified systems where distinct phototroph assemblages occupy the redox stratified chemocline (e.g., Lake Mahoney, Northcote and Hall, 1983; Overmann et al., 1991; Lago di Cadagno, Camacho et al., 2001). Within the chemocline of these systems and presumably FGL, anoxygenic photosynthetic organisms dominate the oxidative arm of the sulfur cycle – oxidizing reduced sulfur species including thiosulfate, sulfide and elemental sulfur producing elemental sulfur or sulfate (Thompson et al., 1990; Zerkle et al., 2010).

Major cations and anions provide a framework for interpreting trace element behavior in the water column. Trends in concentration change of Ca^{2+} and SO_4^{2-}, which are subject to precipitation, dissolution, or biogeochemical transformation, deviated from that of the conservative constituents Na^+ and Cl^-, while Mg^{2+} and HCO_3^- appear to follow the pattern of Na^+ and Cl^-. Specifically, gypsum ($CaSO_4$) is below saturation in the mixolimnion and supersaturated at and below 19 m (SOM Fig. 1), maintaining nearly constant Ca^{2+} and SO_4^{2-} concentrations through the monimolimnion (Fig. 4). TDS is dominated by Ca^{2+} and SO_4^{2-}, and the abrupt increase in TDS that marks the boundary between the bottom of the chemocline and the top of the monimolimnion is due to the increase in those ions.

4.2. Manganese

Manganese is redox sensitive, and is assumed to be delivered to FGL as insoluble manganoan oxides from runoff, settling to the redox transition in the chemocline, where it is reduced to more soluble Mn^{2+}, producing the peak in dissolved Mn concentration at the bottom of the chemocline (Fig. 5). The peak in dissolved Mn observed in both November and July coincides with increased turbidity associated with the microbial plate, and occurs nearly a meter higher in the water column in July compared to November (Fig. 6). The peak in July also exhibits a broader peak with a large shoulder in the oxic zone. The differences in the profile of Mn concentration between November and July may indicate biotic processes or changes in the microbial community that affect Mn chemistry in and near the chemocline. The overlap of O_2 and Mn^{2+} profiles between 15 and 20 m for July implies slow manganese oxidation kinetics. It is generally assumed that Mn oxidation in aquatic environments is driven by biological processes because the kinetics of abiotic oxidation are relatively slow (Tebo et al., 2004).

The overall pattern in dissolved Mn with a peak between the drop in D.O. and increase in ΣS^{2-} is a phenomenon observed in many stratified aquatic systems ranging from fresh to hypersaline (e.g., Paul Lake, Taillefert and Gaillard, 2002; Lago di Cadagno, Tonolla et al., 1998; Lake A, Gibson et al., 2002; Framvaren Fjord, Yao and Millero, 1995; Mariager Fjord, Ramsing et al., 1996; Drammensfjord, Öztürk, 1995; the Black Sea, Lewis and Landing, 1991, Tebo, 1991; Orca Basin, Trefry et al., 1984; Van Cappellen et al., 1998). The peak has been attributed to biologically mediated cycling of insoluble Mn(IV) (as MnO_2) in the oxic zone and soluble $Mn^{2+}_{(aq)}$ in the euxinic zone (Trefry et al., 1984; Tebo, 1991; Van Cappellen et al., 1998; Taillefert and Gaillard, 2002). Mn thus acts as a microbially mediated redox shuttle between the oxic and euxinic zones, with $Mn^{2+}_{(aq)}$ diffusing upward, being oxidized to Mn(IV) or Mn(III) which then settles as MnO_x particulates (where $x \leqslant 2$) to be reduced once again to $Mn^{2+}_{(aq)}$. In support of this hypothesis, peaks in particulate Mn are

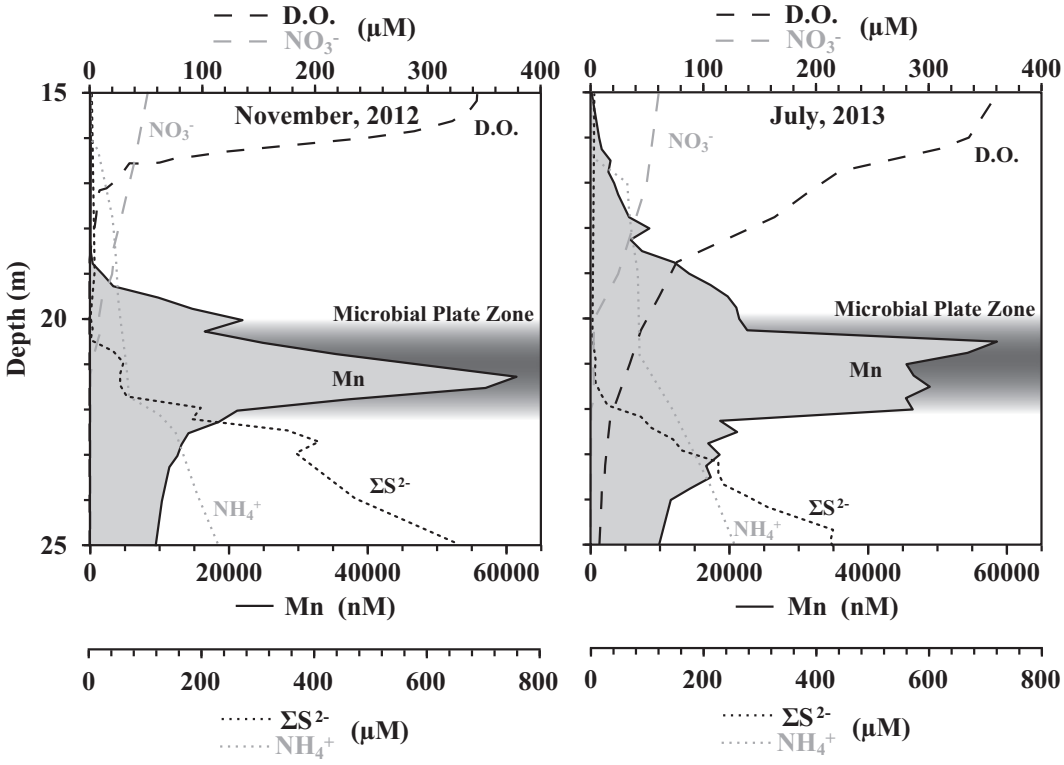

Fig. 6. Zoom in of dissolved Mn, D.O., NO_3^-, ΣS^{2-}, and NH_4^+ concentration for 15–25 m from November, 2012 (left) and July, 2013 (right). Mn is represented by a grey-filled solid black line, D.O. by a black dashed line, NO_3^- by a grey dashed line, ΣS^{2-} by a black dotted line, and NH_4^+ by a grey dotted line. The zone of high turbidity associated with the microbial plate is shown by shaded black box. Note different scales for each analyte.

often found above peaks in dissolved Mn (Trefry et al., 1984; Lewis and Landing, 1991; Öztürk, 1995; Ramsing et al., 1996; Van Cappellen et al., 1998; Tankere et al., 2001; Taillefert and Gaillard, 2002; Yakushev et al., 2009). The rate of Mn^{2+} oxidation is elevated in the presence of bacteria (Hastings and Emerson, 1986). The abrupt decrease in Mn concentration moving up the water column could be indicative of microbially mediated Mn oxidation. Indirect reduction of Mn(IV) driven by microbially-generated sulfide has been observed (Burdige and Nealson, 1986) according to the reaction:

$$MnO_2 + HS^- + 3H^+ => Mn^{2+} + S^0 + H_2O \quad (1)$$

Biologically mediated Mn(IV) reduction coupled to oxidation of reduced sulfur species has also been observed (Aller and Rude, 1988), according to the reactions:

$$4MnO_2 + HS^- + 7H^+ => 4Mn^{2+} + SO_4^{2-} + 4H_2O \quad (2)$$

$$3MnO_2 + S^0 + 4H^+ => 3Mn^{2+} + SO_4^{2-} + 2H_2O. \quad (3)$$

Additionally, Fe^{2+} oxidation has also been linked to Mn reduction (Myers and Nealson, 1988) via the following reactions:

$$MnO_2 + 2Fe^{2+} + 4H^+ => Mn^{2+} + 2Fe^{3+} + 2H_2O \quad (4)$$

$$MnO_2 + 2Fe^{2+} + H_2O => Mn^{2+} + Fe_2O_3 + 2H^+. \quad (5)$$

A sharp peak in S^0 (concentration >30 μM) has been observed at 20.5 m coincident with the increase of sulfide concentrations above detection limits (~1 μM) and a turbidity peak from samples collected in October of 2008 and April of 2009 (Zerkle et al., 2010). Sulfur isotopic analysis indicated S^0 $\delta^{34}S$ values consistent with production via sulfide oxidation by anoxygenic phototrophs. These observations, coupled to the occurrence of the dissolved Mn peak below the onset of euxinia (~20.5 m, defined by ORP and ΣS^{2-} in Fig. 3) suggests the production of S^0 is linked to anoxygenic photosynthesis rather than abiotic reduction of Mn(IV) by HS^- because the peak in Mn^{2+} occurs below the appearance of HS^-. Still, reaction 1 cannot be ruled out. Alternatively, S^0 production can occur via the autocatalytic reduction of HS^- by Mn^{2+} (Morse et al., 1987), according to the following reactions:

$$Mn^{2+} + HS^- + O_2 => Mn^{2+} + S^0 + HO_2^-, \quad (6)$$

and

$$HO_2^- + HS^- => 2OH^- + S^0. \quad (7)$$

Co^{2+} (discussed below) is a more effective catalyst than Mn^{2+}, so an increase of free Co^{2+} would make Co available to drive the autocatalytic conversion of HS^- to S^0 with Co replacing Mn in reaction 6 (Morse et al., 1987), potentially contributing to the creation of S^0 in the chemocline. The diffusion of NH_4^+ from the monimolimnion and NO_3^- from the mixolimnion into the zone of peak dissolved Mn concentration (Fig. 6) suggest biologically mediated Mn(IV) reduction coupled with NH_4^+ oxidation to N_2, and Mn^{2+}

oxidation coupled with NO_3^- reduction to N_2 (Luther et al., 1997) could contribute to Mn cycling in the chemocline via the reactions:

$$3MnO_2 + 2NH_4^+ + 4H^+ => 3Mn^{2+} + N_2 + 6H_2O, \quad (8)$$

and

$$5Mn^{2+} + 2NO_3^- + 8OH^- => 5MnO_2 + N_2 + 4H_2O, \quad (9)$$

In oxygen minimum zones (OMZs) today, low N:P ratios have been interpreted as net fixed-N loss presumably due to denitrification and anaerobic ammonia oxidation (Kuypers et al., 2005; Johnston et al., 2009). In the redoxcline of FGL, biogeochemical cycling of Mn in the chemocline could be a putative net sink for dissolved inorganic nitrogen.

The decrease in dissolved Mn down the water column in the monimolimnion indicates a mechanism of removal/loss. Carbonate precipitation is a greater control on removal of Mn from anoxic water than sulfide, and when present, calcite will serve as a nucleation site for solid solution Mn-Ca-carbonates (Mucci, 2004). Furthermore, manganoan calcite is associated with biological Mn reduction (Aller and Rude, 1988), and up to 75% of Mn in anoxic Black Sea sediments has been found to be associated with the carbonate phase (Kiratli and Ergin, 1996). Calculation of the rhodochrosite ($MnCO_3$) saturation index based on solubility product values from Jensen et al. (2002) indicate saturation to supersaturation conditions are present in the chemocline (Fig. 7) and below. However, large discrepancies exist between the solubility product values from resuspension of rhodochrosite crystals (yielding a lower solubility product) and precipitation from a supersaturated solution (yielding a higher solubility product) (Jensen et al., 2002). Thus, the interpretation of near saturation versus supersaturation of rhodochrosite in the monimolimnion (Fig. 7) varies depending on the K_{sp} used. The continuing decrease in dissolved Mn concentration throughout the water column suggests precipitation of rhodochrosite or a mixed Ca-Mn carbonate such as kutnahorite ($CaMn(CO_3)_2$), supporting the lower solubility product value from Jensen et al. (2002). Given the precipitation of calcite in the oxic zone of FGL as a result of oxygenic phototrophs (including "whiting events"; Thompson et al., 1997), there is presumably a seasonal supply of calcite precipitated by cyanobacteria serving as nucleation sites for precipitation of manganous carbonates as a disordered carbonate phase (Mucci, 2004) throughout the water column. The relatively low concentration of dissolved Mn in sediment pore water (123 nM compared to 4329 nM in the immediately overlying water; Fig. 5) further supports a carbonate sink for Mn consistent with Kiratli and Ergin (1996).

4.3. Iron

The peak in dissolved Fe concentration in the chemocline and elevated dissolved Fe in the sulfidic monimolimnion is presumably due to the reduction of

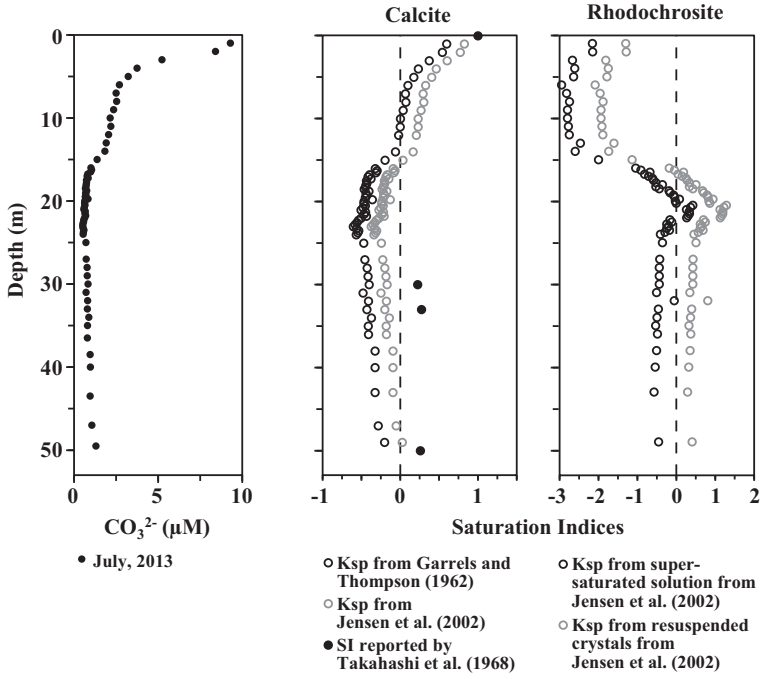

Fig. 7. Calculated concentration of CO_3^{2-} and saturation indices (SI) of calcite ($CaCO_3$) and rhodochrosite ($MnCO_3$) at FGL for samples collected in July, 2013. Calcite SI values are calculated from solubility products (K_{sp}) reported in Garrels and Thompson (1962) (open black circles) and Jensen et al. (2002) (open grey circles), and are plotted with SI values reported for FGL by Takahashi et al. (1968) (closed black circles). Rhodochrosite SI values are calculated based on solubility products determined from precipitation of rhodochrosite from a supersaturated solution (open black circles) or from resuspension of wet rhodochrosite crystals (open grey circles) by Jensen et al. (2002). Dashed line indicates saturation (SI = 0).

insoluble Fe(III) to soluble Fe^{2+}, which is in turn constrained by the presence of sulfide and the potential for formation and precipitation of irons sulfides (Fig. 8). Saturation indices were calculated for metastable iron sulfide minerals (a.k.a. acid volatile sulfides, which are soluble in hot HCl) amorphous iron monosulfide ($FeS_{amorphous}$), mackinawite (FeS), and greigite (Fe_3S_4) using K_{sp} values from Morse et al. (1987), and the proposed amorphous mineral $FeMo_{0.6}S_{2.8}$ using K_{sp} values from Helz et al. (2011) (Fig. 9). While $FeS_{amorphous}$ is undersaturated throughout the water column, greigite and $FeMo_{0.6}S_{2.8}$ (discussed in Section 4.6. below) transitions from undersaturated to supersaturated coincident with the peak in dissolved Fe concentration, and mackinawite approaches saturation near 40 m. Pyrite (FeS_2) is supersaturated throughout the water column (calculations not shown, K_{sp} values from Morse et al., 1987); however, a previous study at FGL showed that little pyrite was formed in the water column, and most was formed diagenetically in the top 15 cm of sediments (Suits and Wilkin, 1998). Pyrite forms according to the reaction:

$$Fe^{2+} + HS^- + S^0 => FeS_2 + H^+. \quad (10)$$

Given the paucity of S^0 in the water column, pyrite precipitation would be inhibited except near the redoxcline where S^0 is produced by anoxygenic phototrophs oxidizing sulfide (Zerkle et al., 2010). The diagenetic formation of pyrite in the sediments suggests a steady source of S^0.

The position of the dissolved Fe peak below that of the dissolved Mn peak is consistent with what has been observed in other stratified systems, including Esthwaite Water (Hamilton-Taylor et al., 2005), Lago di Cadagno (Tonolla et al., 1998), Framvaren Fjord (Jacobs et al., 1985; Haraldsson and Westerlund, 1988), Drammensfjord (Öztürk, 1995), the Black Sea (Haraldsson and Westerlund, 1988; Lewis and Landing, 1991; Tankere et al., 2001), and Orca Basin (Van Cappellen et al., 1998). The location of the peak in dissolved Fe (presumed to be Fe^{2+}) below that of dissolved Mn (presumed to be Mn^{2+}) is consistent with Fe(III) as insoluble oxy-hydroxide particulates, often depicted as $Fe(OH)_3$, settling through the zone of Mn(IV) and Mn(III) reduction to a zone of Fe(III) reduction to Fe^{2+} driven by biologically mediated reduction or abiotic reduction by sulfide. The Fe^{2+} then diffuses down into the euxinic zone where it is scavenged and precipitated as iron sulfides, or upward where it can react with MnO_x to produce Mn^{2+} (via Eqs. (4 and 5)) or be oxidized through biologically mediated processes such as anoxygenic photosynthesis (Ehrenreich and Widdel, 1994) and produce $Fe(OH)_3$ that can again settle back into the zone of Fe(III) reduction. Given the concentration of dissolved Mn is at least an order of magnitude greater than dissolved Fe, the contribution of Fe^{2+} oxidation to MnO_x reduction may be minor compared to the μM to mM concentrations of reduced sulfur species present such as ΣS^{2-} (Figs. 4 and 8), and S^0 and $S_2O_3^{2-}$ (Zerkle et al., 2010). Pore water dissolved Fe concentration was 1131 nM, which is over an order of magnitude higher than the concentration of the immediately overlying water (Fig. 5), indicating dissolution of particulate Fe in the interstitial water. Previous work on

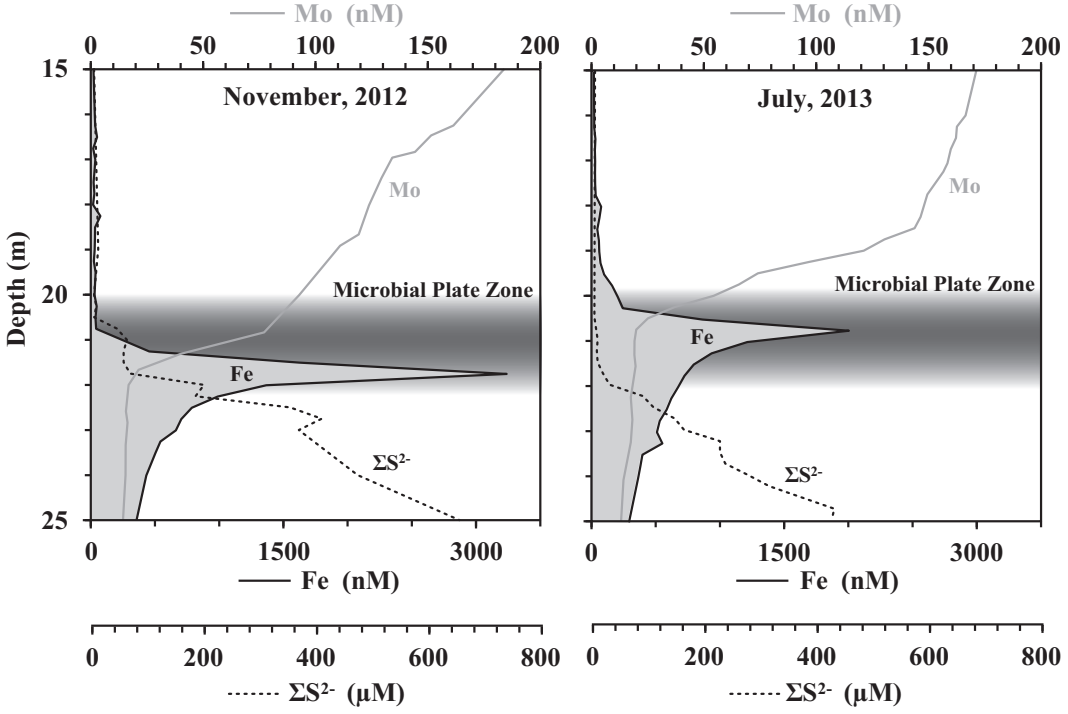

Fig. 8. Zoom in of dissolved Fe, dissolved Mo, and ΣS^{2-} concentration for 15–25 m from November, 2012 (left) and July, 2013 (right). Fe is represented by a grey-filled solid black line, Mo by a solid dark grey line, and ΣS^{2-} by a black dotted line. The zone of high turbidity associated with the microbial plate is shown by a shaded black box. Note different scales for each analyte.

FGL sediments has suggested that iron oxides can settle through the euxinic zone without being fully reduced, with crystalline iron oxides found in the top 17 cm of sediments, and amorphous iron oxides in the top ~3 cm (Suits and Wilkin, 1998). The solubilization of Fe could be due, in large part, to *in situ* reduction of iron oxides and diagenesis of greigite and mackinawite to pyrite, which would also release any elements scavenged from the water column by the iron-sulfide minerals or associated with the iron-oxides. Furthermore, much of the dissolved Fe^{2+} is likely complexed (possibly with sulfides), as the system is oversaturated with respect to pyrite.

4.4. Cobalt

Dissolved Co exhibits a peak in concentration coincident with that of dissolved Mn (Fig. 5). Dissolved Co concentrations mirroring dissolved Mn in pattern and peak location have been reported in many stratified systems (e.g., Framvaren Fjord and Black Sea, Jacobs et al., 1985; Haraldsson and Westerlund, 1988; Lewis and Landing, 1991, 1992; Drammensfjord, Öztürk, 1995; Paul Lake, Taillefert and Gaillard, 2002). Cobalt is found as Co^{2+} in natural waters, and dissolved Co is predominantly present chelated to organic compounds in freshwater (Qian et al., 1998) as well as seawater (Ellwood and van den Berg, 2001), with a sparingly small fraction present as free Co^{2+}. An extensive study of particulate and dissolved Mn and Co at a stratified lake (Paul Lake, MI) indicates intimate coupling of Mn and Co, with dissolved Co scavenged from the oxic zone by particulate MnO_x through adsorption or incorporation, followed by release of dissolved Co coincident with the reduction and dissolution of particulate MnO_x (Taillefert and Gaillard, 2002). Given the tight coupling of dissolved Co to that of dissolved Mn concentration at FGL, it seems reasonable to assume the Paul Lake model applies. The only behavior where Co deviates from that of Mn at FGL is in the pore water, where Co concentration increases to 127 nM (in contrast to the decrease in Mn concentration observed going from monimolimnion to pore water, Fig. 5), suggesting increased Co solubility, possibly due to chelation with organic ligands.

4.5. Nickel

Dissolved Ni exhibits no dramatic change in concentration throughout the FGL water column. The increase in TDS in the anoxic zone at least implies a potential increase in Ni concentration with increasing depth even if Ni is not sensitive to changes in redox or the presence of sulfide. Lack of change from oxic to euxinic water is similar to the results reported for other stratified systems (e.g., Drammensfjord, Öztürk, 1995; Framvaren Fjord and the Black Sea, Jacobs et al., 1985; Haraldsson and Westerlund, 1988; Lewis and Landing, 1992; Yiğiterhan et al., 2011). Earlier studies focused on the effects of sulfide scavenging of Ni and other trace elements from the water column (Jacobs et al., 1985; Lewis and Landing, 1992), but more recent work has demonstrated the importance of Ni complexation with dissolved organic compounds. In circum-neutral waters from lake, river, and groundwater samples with DOC and Ni concentrations similar to FGL (42–358 μM and 4–30 nM, respectively), 99.9% of dissolved Ni was bound to organic ligands (Xue et al., 2001, filter size of 0.45 μm). However, higher concentrations of other divalent cations may effectively compete for complexing sites. For instance, in environmental water samples with Ca^{2+} concentrations of >8 mM, ~90% of dissolved Ni was present as free aquo complex ($Ni(H_2O)_6^{2+}$), with DOC concentrations greater than 292 μM and dissolved Ni concentration >2.1 μM (Mandal et al., 2002, filter size of 0.45 μm). Similar levels of labile Ni (88.6%) have been observed in river water samples (Yebra-Biurrun and Castro-Romero, 2011). The DOC concentration in FGL is ~160 μM throughout the water column (SOM Fig. 2), thus the Ni/DOC ratio is constant. Under these conditions, coupled to the relatively high average concentration of Ca^{2+} observed in the mixolimnion and monimolimnion, (11.2 and 15.0 mM, respectively, Fig. 3), dissolved Ni in FGL is expected to be in the $Ni(H_2O)_6^{2+}$ form. This form of Ni, at least under the FGL-like conditions, is apparently unaffected by dramatic changes in redox through the water column. We hypothesize that the groundwater dissolved Ni input is so low as to have a negligible effect on the dissolved Ni in FGL, and that all of the dissolved Ni is associated with DOC (sourced from organic matter input into FGL), such that the dissolved Ni is at a 'steady state' that maintains Ni concentration at ~91 nM throughout the water column. In the sulfide-rich pore water, dissolved Ni concentration at FGL (767 nM) is elevated compared to the water column concentration (Fig. 5). This observation supports the hypothesis that free Ni may be stabilized by high sulfide concentrations (Calvert and Pedersen, 1993), and while not a dominant process, minor scavenging of dissolved Ni by iron-sulfide precipitates may occur in the euxinic water (Öztürk, 1995), potentially serving as a means for transporting Ni to the sediments where it may be released during the transformation of iron sulfide precipitates to pyrite.

4.6. Molybdenum

The concentration profile of Mo is consistent with those determined for other stratified systems (e.g., Lago di Codagno, Dahl et al., 2010; Rogoznica Lake, Helz et al., 2011; Framvaren Fjord and the Black Sea, Emerson and Huested, 1991), with the highest concentrations observed in the oxic zone and a sharp transition to much lower concentrations in the euxinic zone (Fig. 5). Wang et al. (2011) proposed a model for Mo(VI) conversion to Mo(IV) through reactions with elemental sulfur and potentially via a Mo(V) intermediate, involving the replacement of oxyanion oxygens with sulfides (proposed by Erickson and Helz, 2000). In this model, Mo(VI) diffuses as $Mo^{VI}O_4^{2-}$ from the upper oxic zone to the euxinic monimolimnion where a transition "action point" (ΣS^{2-} >11 μM) is reached and sulfides replace oxygens in $Mo^{VI}O_4^{2-}$ (Erickson and Helz, 2000). Conversion to oxy-thiols occurs nearly immediately according to the reaction:

$$Mo^{VI}O_4^{2-} + H_2S \Rightarrow Mo^{VI}O_3S^{2-} + H_2O \quad (11)$$

once the action point is reached (Erickson and Helz, 2000). Successive replacement occurs on the order of minutes (to $Mo^{VI}O_2S_2^{2-}$), hours (to $Mo^{VI}OS_3^{2-}$) and days (to thiomolybdate, or $Mo^{VI}S_4^{2-}$) (Erickson and Helz, 2000). A reported maximum S^0 concentration (over 30 μM) at 20.5 m in FGL (reported in Zerkle et al., 2010) coincides with an increase in ΣS^{2-} concentration above background levels (>10 μM). Polysulfides form during the oxidation of aqueous sulfide at pH of 7.0 ± 0.4 (Chen and Gupta, 1973) via the reaction:

$$S^{2-} + nS^0 => S_{n+1}^{2-} \quad (12)$$

Elemental sulfur could react with polysulfides forming in the euxinic-oxic convergence zone, and those polysulfides can act as catalysts in the reduction of Mo(VI) oxy-thiomolybdate into Mo(IV) oxy-thiol/thiols (Vorlicek et al., 2004) according to the reaction:

$$Mo^{VI}OS_3^{2-} + \frac{n}{8}S_{8(aq)} => Mo^{IV}OS_{3+n}^{2-} \quad (13)$$

Also, Mo(VI) oxy-thiomolybdate could be reduced to monomers and dimers of Mo(V) oxy-thiols/thiols via:

$$2Mo^{VI}OS_3^{2-} + \frac{n}{8}S_{8(aq)} + H^+ => Mo_2^{V}O_2S_{5+n}^{2-} + HS^-, \quad (14)$$

which disproportionates upon reaction with HS^- to form Mo(VI) and Mo(IV) oxy-thiols/thiols according to the reaction:

$$Mo_2^{V}O_2S_{5+n}^{2-} + HS^- => Mo^{VI}OS_3^{2-} + Mo^{IV}OS_{3+n}^{2-} + H^+. \quad (15)$$

At FGL, the decrease in dissolved Mo concentration is coincident with the peak in dissolved Fe concentration (Fig. 8) and near the transition to supersaturation for the metastable iron sulfide mineral greigite (Fig. 9). This observation suggests that the addition of reactive thiols to Mo(VI), or conversion of Mo(VI) to Mo(IV) facilitates scavenging of Mo from the water column by greigite and/or pyrite. An alternative means for removal of dissolved Mo from sulfidic water has been proposed recently (Helz et al., 2011). In this mechanism, $FeMo_{0.6}S_{2.8}$ forms from the interaction of Fe^{2+} with $Mo^{VI}S_4^{2-}$ and H_2S according to the reaction:

$$Fe^{2+} + 0.6Mo^{VI}S_4^{2-} + 0.4H_2S => FeMo_{0.6}S_{2.8} + 0.8H^+. \quad (16)$$

Speciation for Mo^{VI} anions was calculated for the July, 2013 FGL water column using K values reported by Erickson and Helz (2000). The results of these calculations indicate $Mo^{VI}O_4^{2-}$ and $Mo^{VI}S_4^{2-}$ concentrations are equal at ~20.75 m (Fig. 10). This depth coincides with (*i*) an increase in total sulfide concentration above the 11 μM action point (from 8.3 to 17.8 μM), (*ii*) a decrease in total dissolved Mo concentration, which then stabilizes in the monimolimnion, (*iii*) a peak in iron concentration, and (*vi*) supersaturation of the proposed mineral $FeMo_{0.6}S_{2.8}$. The point of supersaturation of $FeMo_{0.6}S_{2.8}$ occurs half a meter higher in the water column than greigite. Collectively, these data suggest removal of dissolved Mo from the water column is controlled by the geochemical factors governing $FeMo_{0.6}S_{2.8}$ precipitation. Whether by adsorption onto iron sulfides or by precipitation of $FeMo_{0.6}S_{2.8}$ (or a combination of both processes), the net scavenging effect contributes to a ~94% decline in dissolved Mo concentration relative to the mixolimnion, which is similar to the Black Sea (94%, Emerson and Huested, 1991) and Rogoznica Lake (96%, Helz et al., 2011), and greater than other stratified systems (Emerson and Huested, 1991; Dahl et al., 2010). The presence of detectable levels of dissolved Mo throughout the FGL water column further support the findings of Wang et al. (2011), who demonstrated solubilization of Mo(VI) as $Mo^{VI}S_4^{2-}$ during re-oxidation of previously reduced

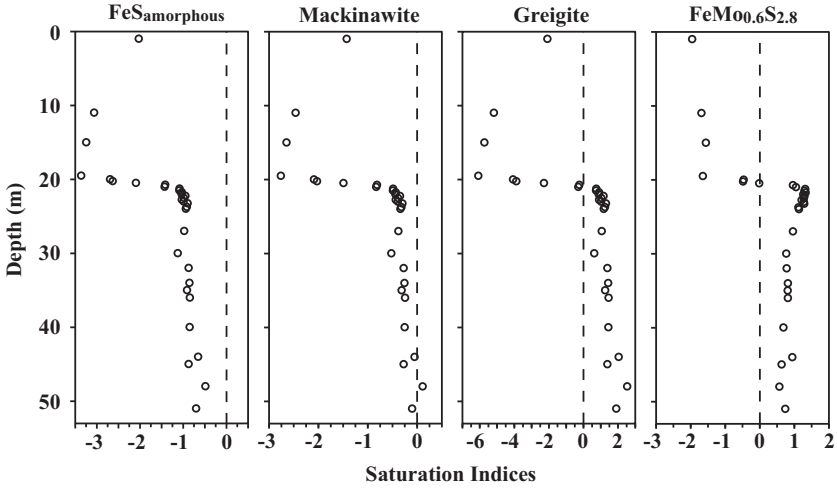

Fig. 9. Saturation indices of amorphous FeS, mackinawite, greigite, and an amorphous $FeMo_{0.6}S_{2.8}$ mineral (proposed by Helz et al., 2011) at FGL from samples collected in July, 2013. Values for amorphous FeS, mackinawite, and greigite were calculated based on solubility products reported by Morse et al. (1987). Values for amorphous $FeMo_{0.6}S_{2.8}$ based on solubility products reported in Erickson and Helz (2000) and Helz et al. (2011). Dashed lines indicate saturation (SI = 0).

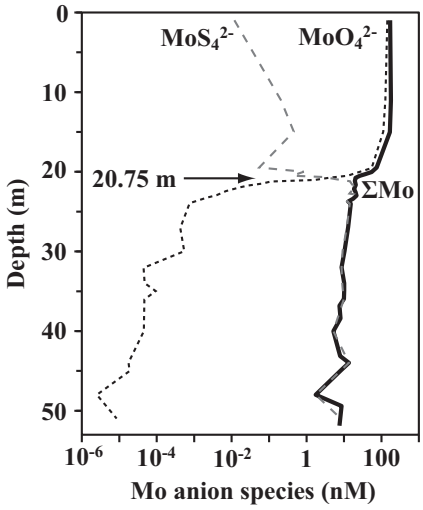

Fig. 10. Calculated and measured concentration of dissolved molybdenum in the water column. Calculated molybdenum oxyanion (MoO_4^{2-}, black dotted line) and thiolanion (MoS_4^{2-}, grey dashed line) determined from *K* values reported in Erickson and Helz (2000). Measured total dissolved molybdenum (ΣMo) indicated with a solid black line.

sediments. Furthermore, $Mo^{VI}S_4^{2-}$ was found to be thermodynamically stabile in experiments where ΣS^{2-} concentration is high enough to destabilize $Mo^{VI}O_4^{2-}$ (Vorlicek et al., 2004). The concentration of dissolved Mo in the sulfide-rich pore water at FGL was 763 nM, four times greater than the values found in the oxic mixolimnion (Fig. 5), and similar to pore water enrichment of dissolved Mo in euxinic lake sediments previously described (Dahl et al., 2010). This suggests remobilization of Mo during diagenesis of Mo-bearing iron-sulfide precipitates into pyrite, consistent with recent findings that 80–100% of Mo in modern and ancient samples formed under sulfidic conditions was not associated with pyrite crystals, but rather the surrounding non-pyritic matrix (Chappaz et al., 2014).

5. TRACE ELEMENT CONCEPTUAL MODEL

FGL may serve as a useful proxy for past redox conditions on Earth. Understanding the conditions under which uptake and incorporation of biologically important trace elements in such systems provides us with a framework for elucidating when primitive metalloenzymes may have first evolved. A conceptual 1-dimensional model summarizing the results of analyses at FGL proposes three distinct zones (Fig. 11). These are: zone 1 – the oxic mixolimnion, zone 2 – the transition between oxic and euxinic water at the chemocline demarked by the peak in turbidity resulting from a dense microbial assemblage, and zone 3 – the perennially euxinic monimolimnion and sulfidic sediments.

Zone 1 (surface to 15 m depth) has dissolved oxygen levels at or above saturation, favoring oxidized forms of Mn, Fe, and Mo, resulting in low dissolved Mn and Fe concentrations and high dissolved Mo (Fig. 5). This zone is similar to the modern ocean, with Fe and Mn potentially acting as limiting nutrients, and abundant Mo bioavailable for Mo-containing enzymes such as those necessary for nitrogen fixation or and nitrate assimilation.

Zone 2 (15–21 m depth) represents the redox transition where Fe, Mo, and to a lesser extent Mn, are removed from the water column and transported to the sediments. Elevated dissolved Mn and Fe concentrations likely result from microbially mediated reduction of MnO_x and $Fe(OH)_3$ settling from the oxic zone and cycling between reduced and oxidized states. A steady advective/diffusive supply of sulfide from the action of sulfate reducing bacteria in the sediments and lower water column maintains anoxic to euxinic conditions, and supports a microbial plate that contains anoxygenic phototrophs, evidenced by the presence of BChl *a* and BChl *e* (Hunter, 2012), which contribute to Fe-cycling (Fe^{2+} oxidation) and ΣS^{2-} oxidation/S^0 generation. The iron-sulfide mineral greigite becomes supersaturated, leading to precipitation from the water column along with pyrite (dependent upon the presence of S^0). Dissolved Mo concentration drops due to replacement of oxygens with sulfides on molybdenum oxyanions and subsequent scavenging through precipitation of $FeMo_{0.6}S_{2.8}$ and/or absorption to iron-sulfide precipitates, transporting Mo to the sediments. Rhodochrosite ($MnCO_3$) becomes supersaturated and precipitates (either as $MnCO_3$, or as a $CaMn(CO_3)_2$ mixed phase) onto $CaCO_3$ settling down from the oxic zone, which is subsequently transported to the sediments.

Zone 3 (below 21 m) consists of the perennially euxinic monimolimnion and sulfidic sediments. Mn and Fe are enriched in the euxinic water and diffuse upward to feed the cycling in Zone 2, and are ultimately transported as precipitates to the sediments. Sulfate reduction in the sediments and water column maintain euxinic conditions in the monimolimnion. The stratified character of the water column and the metabolic activities of the microbial communities act as effective catalysts for transport of trace elements to the sediments, where diagenesis releases some as dissolved constituents of the pore water. The overlying stratified water column affords the opportunity for transport to and enrichment of essential trace elements in the sediments.

6. POTENTIAL EARLY EARTH IMPLICATIONS

FGL may help elucidate the effects of Proterozoic ocean stratification on trace element behavior. Due to the continuous input of sulfate from groundwater that passes through gypsum-bearing shale, FGL maintains sulfate concentrations throughout the water column that are similar to what is thought to have been present during the Proterozoic (Schröder et al., 2008; Planavsky et al., 2012), and sustain bacterial sulfate reduction to produce euxinic conditions in the monimolimnion. Euxinic deep ocean water is thought to have been prevalent from 0.7 to 1.8 Ga, and possibly back to the great oxidation event circa 2.45 Ga (Lyons et al., 2009). Similar to modern OMZs, the photic zone of stratified regions of Proterozoic oceans are thought to have had persistently low levels of fixed N, driving the need for biological nitrogen fixation (Johnston et al., 2009). The data presented here also underscore an overlooked role

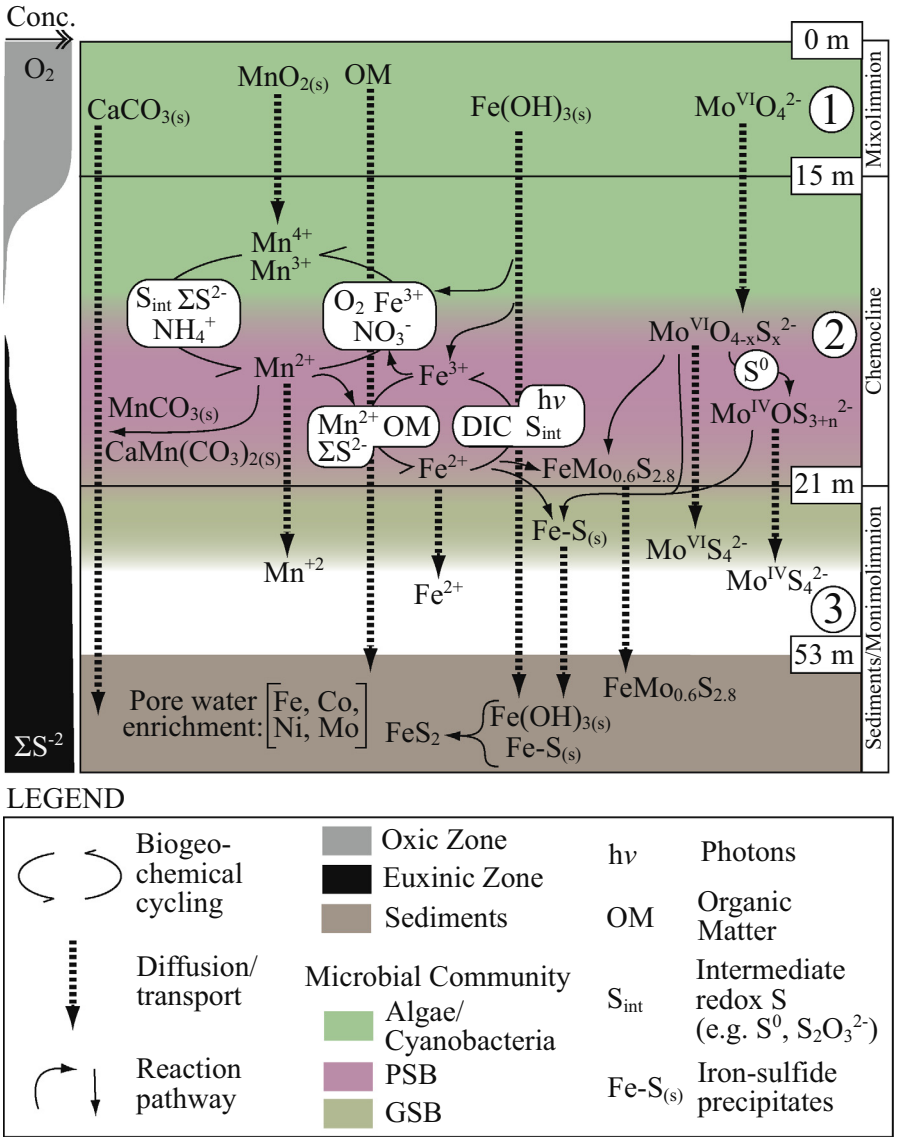

Fig. 11. Conceptual model for trace element movement at FGL. The oxic mixolimnion (1) supplies oxidized Mn, Fe, and Mo, as well as $CaCO_3$ produced by the action of cyanobacteria, to the transition zone (2). The transition zone (2) is occupied by a diverse microbial community (including cyanobacteria, as well as anoxygenic phototrophs purple sulfur bacteria (PSB) and green sulfur bacteria (GSB)) that actively cycle Mn and Fe between oxidized and reduced forms, producing peaks in dissolved Mn and dissolved Fe. Reduced iron (Fe^{2+}) reacts with sulfide (ΣS^{2-}) to form iron-sulfide precipitates (Fe-$S_{(s)}$). Molybdenum (as the oxyanion molybdate) interacts with sulfide (ΣS^{2-}) and elemental sulfur (S^0) to form Mo^{IV} and Mo^{VI} anions with thiol groups, which can precipitate as $FeMo_{0.6}S_{2.8}$ or sorb to Fe-$S_{(s)}$ and be scoured from the water column and transported to the sediments. Reduced Mn (Mn^{2+}) precipitates onto calcite ($CaCO_3$) as rhodochrosite ($MnCO_3$) or mixed phase $CaMn(CO_3)_2$, and is transported to the sediments. In the sulfidic zone (3), sediment pore water is enriched in elements over the monimolimnion, in part due to release during breakdown of organic matter and during diagenesis of iron precipitates to pyrite (FeS_2).

for Mn (and Fe) cycling in stratified water columns as a sink for fixed nitrogen (e.g., via reactions 8 and 9). In contrast to this model of euxinic zones of Proterozoic oceans, the water column of FGL is replete with fixed N (~60 μM NO_3^- in the surface waters and 100–800 μM NH_4^+ in and below the chemocline). Low dissolved Mo concentrations under sulfide-rich conditions in the Proterozoic oceans are often cited as a barrier to the bioavailability of Mo and thus limiting to key processes in the nitrogen cycle such as nitrogen fixation and assimilatory/dissimilatory nitrate reduction (Anbar and Knoll, 2002; Reinhard et al., 2013). Tracking dissolved Mo concentration through the FGL water column provides evidence for the availability of dissolved Mo, an important factor if fixed N were limiting. Dissolved Mo concentration is nearly double that of modern ocean levels in the mixolimnion (⩾170 nM), and drops to ~20 nM at 21 m, coincident with the turbidity peak due to the anoxygenic phototroph microbial plate, and reaching minimum levels (circum 10 nM) at the bottom of the monimolimnion. In fixed N-limited cultures of the

model diazotroph *Azotobacter vinelandii*, Mo concentrations less than 21 nM repress transcription of *nif*, selecting for expression of one of the alternative forms of the enzyme (Becking, 1962; Jacobson et al., 1986). However, laboratory experiments with diazotrophic cyanobacteria indicate depressed rates of N_2-fixation when Mo concentration drops below 10 nM (Fay and de Vasconcelos, 1974; Jacobs and Lind, 1977; Zahalak et al., 2004; Zerkle et al., 2006; Glass et al., 2010). In light of these studies, it is not apparent that the levels of dissolved Mo would have limited Mo-dependent biological nitrogen fixation in the Proterozoic ocean, assuming oxic and euxinic stratified conditions similar to FGL. These data highlight the need to better constrain the biological demands for Mo under fixed N-limiting conditions similar to Proterozoic oceans. Furthermore, little work has been done on the bioavailability of thiol-containing molybdenum anions or amorphous Mo-containing iron-sulfides, demonstrating a need for pure culture laboratory work to elucidate answers to these questions.

7. CONCLUSIONS

FGL provides a natural laboratory for characterizing the behavior of trace elements in a stratified aqueous environment which transitions from an upper oxic mixolimnion to a lower euxinic monimolimnion. The results also support the mechanism for removal of dissolved Mo from the water column via precipitation of the $FeMo_{0.6}S_{2.8}$ mineral proposed by Helz et al. (2011). Elevated concentrations of trace metals in the sediment pore water suggest that mobilization (indicated by pore water concentrations that greatly exceed that of the overlying monimolimnion) occurs in the interstitial fluids for Fe, Co, Ni, Mo, but not for Mn. Thus, a stratified water body is effective at transporting essential elements to the sediments where they are available in relatively high concentrations. Due to the unique conditions that maintain stratification and high sulfide concentration from continuous sulfate input driving biological sulfate reduction, FGL can serve as an analog to the redox conditions that may have been prevalent in the Proterozoic following the great oxidation event when the ocean was flushed with sulfate as atmospheric oxygen oxidized labile sulfides on the continents. As such, conditions at FGL suggest Mn and Fe cycling within the chemocline, Mo removal from the euxinic zone, and dissolved trace metal enrichment in sediment pore water were possible conditions in Proterozoic oceans.

ACKNOWLEDGEMENTS

The authors thank Hamilton College students Rachel Green, Daniel Licthenauer, Matthew Bzurstoski, Kevin Boettger, Robert Clayton, Helen Farrell, Leonard Kilekwang, Christopher Rider and Andrew Seraichick for their assistance during sample collection and processing, the Hamilton College Dean of Faculty for providing student summer research stipends, Bruce Wegter for operating the Hamilton College research boat, the New York State Parks, the Green Lakes State Park staff and Ranger in particular for their help, and the NASA Astrobiology Institute, the Penn State Astrobiology Research Center, the NASA Postdoctoral Program, and NSF Grant EAR-1349258 for their generous support. T.L.H. graciously acknowledges support from the NAI Postdoctoral Program. J.R.H. would like to thank Chris House for his encouragement and helpful conversations, and PSU student Brianna McClure for her assistance during sample collection and processing. The authors also wish to thank Christopher Reinhard and an anonymous reviewer for valuable insights and constructive criticism that improved this manuscript.

APPENDIX A. SUPPLEMENTARY DATA

Supplementary data associated with this article can be found, in the online version, at http://dx.doi.org/10.1016/j.gca.2015.06.024.

REFERENCES

Aller R. C. and Rude P. D. (1988) Complete oxidation of solid phase sulfides by manganese and bacteria in anoxic marine sediments. *Geochim. Cosmochim. Acta* **52**(3), 751–765.

Anbar A. D. and Knoll A. H. (2002) Proterozoic ocean chemistry and evolution: a bioinorganic bridge? *Science* **297**(5584), 1137–1142.

Arnold G. L., Anbar A. D., Barling J. and Lyons T. W. (2004) Molybdenum isotope evidence for widespread anoxia in mid-Proterozoic oceans. *Science* **304**(5667), 87–90.

Becking J. H. (1962) Species differences in molybdenum and vanadium requirements and combined nitrogen utilization by Azotobacteriaceae. *Plant Soil* **16**(2), 171–201.

Brunskill G. J. and Ludlam S. D. (1969) Fayetteville Green Lake, New York. I. Physical and chemical limnology. *Limnol. Oceanogr.* **14**(6), 817–829.

Burdige D. J. and Nealson K. H. (1986) Chemical and microbiological studies of sulfide-mediated manganese reduction. *Geomicrobiol. J.* **4**(4), 361–387.

Calvert S. E. and Pedersen T. F. (1993) Geochemistry of recent oxic and anoxic marine sediments: implications for the geological record. *Mar. Geol.* **113**(1), 67–88.

Camacho A., Erez J., Chicote A., Florín M., Squires M. M., Lehmann C. and Backofen R. (2001) Microbial microstratification, inorganic carbon photoassimilation and dark carbon fixation at the chemocline of the meromictic Lake Cadagno (Switzerland) and its relevance to the food web. *Aquat. Sci.* **63**(1), 91–106.

Cappenberg T. E. (1974) Interrelations between sulfate-reducing and methane-producing bacteria in bottom deposits of a freshwater lake. I. Field observations. *Antonie Van Leeuwenhoek* **40**(2), 285–295.

Chappaz A., Lyons T. W., Gregory D. D., Reinhard C. T., Gill B. C., Li C. and Large R. R. (2014) Does pyrite act as an important host for molybdenum in modern and ancient euxinic sediments? *Geochim. Cosmochim. Acta* **126**, 112–122.

Chen K. Y. and Gupta S. K. (1973) Formation of polysulfides in aqueous solution. *Environ. Lett.* **4**(3), 187–200.

Cline J. D. (1969) Spectrophotometric determination of hydrogen sulfide in natural waters. *Limnol. Oceanogr.* **14**, 454–458.

Collier R. W. (1985) Molybdenum in the northeast Pacific Ocean. *Limnol. Oceanogr.* **30**(6), 1351–1354.

Dahl T. W., Anbar A. D., Gordon G. W., Rosing M. T., Frei R. and Canfield D. E. (2010) The behavior of molybdenum and its isotopes across the chemocline and in the sediments of sulfidic Lake Cadagno, Switzerland. *Geochim. Cosmochim. Acta* **74**(1), 144–163.

Deevey E. S., Nakai N. and Stuiver M. (1963) Fractionation of sulfur and carbon isotopes in a meromictic lake. *Science* **139**(3553), 407-407.

Dupont C. L., Butcher A., Valas R. E., Bourne P. E. and Caetano-Anollés G. (2010) History of biological metal utilization inferred through phylogenomic analysis of protein structures. *PNAS* **107**(23), 10567–10572.

Eggleton F. E. (1931) A limnological study of the profundal bottom fauna of certain fresh-water lakes. *Ecol. Monogr.* **1**(3), 232–331.

Eggleton F. E. (1956) Limnology of a meromictic, interglacial, plunge-basin lake. *Trans. Am. Microsc. Soc.*, 334–378.

Ehrenreich A. and Widdel F. (1994) Anaerobic oxidation of ferrous iron by purple bacteria, a new type of phototrophic metabolism. *Appl. Environ. Microbiol.* **60**(12), 4517–4526.

Ellwood M. J. and van den Berg C. M. (2001) Determination of organic complexation of cobalt in seawater by cathodic stripping voltammetry. *Mar. Chem.* **75**(1), 33–47.

Emerson S. R. and Huested S. S. (1991) Ocean anoxia and the concentrations of molybdenum and vanadium in seawater. *Mar. Chem.* **34**(3), 177–196.

Erickson B. E. and Helz G. R. (2000) Molybdenum(VI) speciation in sulfidic waters: stability and lability of thiomolybdates. *Geochim. Cosmochim. Acta* **64**(7), 1149–1158.

Fay P. and de Vasconcelos L. (1974) Nitrogen metabolism and ultrastructure in *Anabaena cylindrica*. *Arch. Microbiol.* **99**(1), 221–230.

Fry B. (1986) Sources of carbon and sulfur nutrition for consumers in three meromictic lakes of New York State. *Limnol. Oceanogr.* **31**(1), 79–88.

Garrels R. M. and Thompson M. E. (1962) A chemical model for sea water at 25 degrees C and one atmosphere total pressure. *Am. J. Sci.* **260**(1), 57–66.

Gibson J. A., Vincent W. F., Van Hove P., Belzile C., Wang X. and Muir D. (2002) Geochemistry of ice-covered, meromictic Lake A in the Canadian High Arctic. *Aquat. Geochem.* **8**(2), 97–119.

Glass J. B., Wolfe-Simon F., Elser J. J. and Anbar A. D. (2010) Molybdenum-nitrogen co-limitation in freshwater and coastal heterocystous cyanobacteria. *Limnol. Oceanogr.* **55**(2), 667.

Hamilton-Taylor J., Smith E. J., Davison W. and Sugiyama M. (2005) Resolving and modeling the effects of Fe and Mn redox cycling on trace metal behavior in a seasonally anoxic lake. *Geochim. Cosmochim. Acta* **69**(8), 1947–1960.

Hamilton-Taylor J. and Davison W. (1995) Redox-driven cycling of trace elements in lakes. In *Physics and Chemistry of Lakes*. Springer, Berlin Heidelberg, pp. 217–263.

Haraldsson C. and Westerlund S. (1988) Trace metals in the water columns of the Black Sea and Framvaren Fjord. *Mar. Chem.* **23**(3), 417–424.

Hastings D. and Emerson S. (1986) Oxidation of manganese by spores of a marine bacillus: kinetic and thermodynamic considerations. *Geochim. Cosmochim. Acta* **50**(8), 1819–1824.

Helz G. R., Bura-Nakić E., Mikac N. and Ciglenečki I. (2011) New model for molybdenum behavior in euxinic waters. *Chem. Geol.* **284**(3), 323–332.

Hilfinger, IV, M. F., Mullins H. T., Burnett A. and Kirby M. E. (2001) A 2500 year sediment record from Fayetteville Green Lake, New York: evidence for anthropogenic impacts and historic isotope shift. *J. Paleolimnol.* **26**(3), 293–305.

Hunter, S. E. (2012). Spatio-temporal Variability in the Phototrophic Chemocline Community at Fayetteville Green Lake (New York). M.S. thesis, Pennsylvania State Univ.

Jacobs L., Emerson S. and Skei J. (1985) Partitioning and transport of metals across the O_2/H_2S interface in a permanently anoxic basin: Framvaren Fjord, Norway. *Geochim. Cosmochim. Acta* **49**(6), 1433–1444.

Jacobs R. and Lind O. (1977) The combined relationship of temperature and molybdenum concentration to nitrogen fixation by *Anabaena cylindrica*. *Microb. Ecol.* **3**(3), 205–217.

Jacobson M. R., Premakumar R. and Bishop P. E. (1986) Transcriptional regulation of nitrogen fixation by molybdenum in *Azotobacter vinelandii*. *J. Bacteriol.* **167**(2), 480–486.

Jelacic, A. J. (1970). Physical limnology of Green and Round Lakes. Fayetteville, New York. Ph. D. thesis, Univ. of Rochester.

Jensen D. L., Boddum J. K., Tjell J. C. and Christensen T. H. (2002) The solubility of rhodochrosite ($MnCO_3$) and siderite ($FeCO_3$) in anaerobic aquatic environments. *Appl. Geochem.* **17**(4), 503–511.

Johnston D. T., Wolfe-Simon F., Pearson A. and Knoll A. H. (2009) Anoxygenic photosynthesis modulated proterozoic oxygen and sustained earth's middle age. *PNAS* **106**(40), 16925–16929.

Kiratli N. and Ergin M. (1996) Partitioning of heavy metals in surface Black Sea sediments. *Appl. Geochem.* **11**(6), 775–788.

Kump L. R., Pavlov A. and Arthur M. A. (2005) Massive release of hydrogen sulfide to the surface ocean and atmosphere during intervals of oceanic anoxia. *Geology* **33**(5), 397–400.

Kuypers M. M., Lavik G., Woebken D., Schmid M., Fuchs B. M., Amann R., Jørgensen B. B. and Jetten M. S. (2005) Massive nitrogen loss from the Benguela upwelling system through anaerobic ammonium oxidation. *PNAS* **102**(18), 6478–6483.

Lamers L. P., Tomassen H. B. and Roelofs J. G. (1998) Sulfate-induced eutrophication and phytotoxicity in freshwater wetlands. *Environ. Sci. Technol.* **32**(2), 199–205.

Lewis B. L. and Landing W. M. (1991) The biogeochemistry of manganese and iron in the Black Sea. *Deep Sea Res. Part A: Oceanogr. Res. Pap.* **38**, S773–S803.

Lewis B. L. and Landing W. M. (1992) The investigation of dissolved and suspended-particulate trace metal fractionation in the Black Sea. *Mar. Chem.* **40**(1), 105–141.

Lovley D. R. and Klug M. J. (1983) Sulfate reducers can outcompete methanogens at freshwater sulfate concentrations. *Appl. Environ. Microbiol.* **45**(1), 187–192.

Luther, III, G. W., Sundby B., Lewis B. L., Brendel P. J. and Silverberg N. (1997) Interactions of manganese with the nitrogen cycle: alternative pathways to dinitrogen. *Geochim. Cosmochim. Acta* **61**(19), 4043–4052.

Lyons T. W., Anbar A. D., Severmann S., Scott C. and Gill B. C. (2009) Tracking euxinia in the ancient ocean: a multiproxy perspective and proterozoic case study. *Annu. Rev. Earth Planet Sci.* **37**, 507–534.

Mandal R., Hassan N. M., Murimboh J., Chakrabarti C. L., Back M. H., Rahayu U. and Lean D. R. (2002) Chemical speciation and toxicity of nickel species in natural waters from the Sudbury area (Canada). *Environ. Sci. Technol.* **36**(7), 1477–1484.

McCormick M. L., Banishki N., Powell S., Rumack A. and Garrett J. M. (2014) A low cost multi-level sampling device for synchronous aseptic collection of environmental water samples. *J. Microbiol. Methods* **105**, 51–53.

Meyer K. M. and Kump L. R. (2008) Oceanic euxinia in earth history: causes and consequences. *Annu. Rev. Earth Planet. Sci.* **36**, 251–288.

Morse J. W., Millero F. J., Cornwell J. C. and Rickard D. (1987) The chemistry of the hydrogen sulfide and iron sulfide systems in natural waters. *Earth-Sci. Rev.* **24**(1), 1–42.

Mucci A. (2004) The behavior of mixed Ca–Mn carbonates in water and seawater: controls of manganese concentrations in marine porewaters. *Aquat. Geochem.* **10**(1–2), 139–169.

Muller E. H. (1967) Geologic setting of Green and Round Lakes near Fayetteville, New York. In *Some aspects of meromixis*.

Syracuse University, Department of Civil Engineering, Syracuse, New York, pp. 96–121.

Murray J. W. (1987) Mechanisms controlling the distribution of trace elements in oceans and lakes. In *Sources and Fates of Aquatic Pollutants* (eds. R. A. Hites, S. J. Eisenreich). American Chemical Society, Washington, D.C., pp. 153–184.

Myers C. R. and Nealson K. H. (1988) Microbial reduction of manganese oxides: interactions with iron and sulfur. *Geochim. Cosmochim. Acta* **52**(11), 2727–2732.

Northcote T. G. and Hall K. J. (1983) Limnological contrasts and anomalies in two adjacent saline lakes. *Hydrobiologia* **105**(1), 179–194.

Oduro H., Kamyshny, Jr, A., Zerkle A. L., Li Y. and Farquhar J. (2013) Quadruple sulfur isotope constraints on the origin and cycling of volatile organic sulfur compounds in a stratified sulfidic lake. *Geochim. Cosmochim. Acta* **120**, 251–262.

Overmann J., Beatty J. T., Hall K. J., Pfennig N. and Northcote T. G. (1991) Characterization of a dense, purple sulfur bacterial layer in a meromictic salt lake. *Limnol. Oceanogr.*, 846–859.

Öztürk M. (1995) Trends of trace metal (Mn, Fe Co, Ni, Cu, Zn, Cd and Pb) distributions at the oxic–anoxic interface and in sulfidic water of the Drammensfjord. *Mar. Chem.* **48**(3), 329–342.

Planavsky N. J., Bekker A., Hofmann A., Owens J. D. and Lyons T. W. (2012) Sulfur record of rising and falling marine oxygen and sulfate levels during the Lomagundi event. *PNAS* **109**(45), 18300–18305.

Planavsky N. J., McGoldrick P., Scott C. T., Li C., Reinhard C. T., Kelly A. E., Chu X., Bekker A., Love G. D. and Lyons T. W. (2011) Widespread iron-rich conditions in the mid-Proterozoic ocean. *Nature* **477**(7365), 448–451.

Poulton S. W. and Canfield D. E. (2011) Ferruginous conditions: a dominant feature of the ocean through earth's history. *Elements* **7**(2), 107–112.

Qian J., Xue H. B., Sigg L. and Albrecht A. (1998) Complexation of cobalt by natural ligands in freshwater. *Environ. Sci. Technol.* **32**(14), 2043–2050.

Ramsing N. B., Fossing H., Ferdelman T. G., Andersen F. and Thamdrup B. (1996) Distribution of bacterial populations in a stratified fjord (Mariager Fjord, Denmark) quantified by in situ hybridization and related to chemical gradients in the water column. *Appl. Environ. Microbiol.* **62**(4), 1391–1404.

Reinhard C. T., Planavsky N. J., Robbins L. J., Partin C. A., Gill B. C., Lalonde S. V., Bekker A., Konhauser K. O. and Lyons T. W. (2013) Proterozoic ocean redox and biogeochemical stasis. *PNAS* **110**(14), 5357–5362.

Rouxel O. J., Bekker A. and Edwards K. J. (2005) Iron isotope constraints on the Archean and Paleoproterozoic ocean redox state. *Science* **307**(5712), 1088–1091.

Saito M. A., Sigman D. M. and Morel F. M. (2003) The bioinorganic chemistry of the ancient ocean: the co-evolution of cyanobacterial metal requirements and biogeochemical cycles at the Archean–Proterozoic boundary? *Inorg. Chim. Acta* **356**, 308–318.

Schröder S., Bekker A., Beukes N. J., Strauss H. and Van Niekerk H. S. (2008) Rise in seawater sulphate concentration associated with the Paleoproterozoic positive carbon isotope excursion: evidence from sulphate evaporites in the ~2.2–2.1 Gyr shallow-marine Lucknow Formation, South Africa. *Terra Nova* **20**(2), 108–117.

Scott C., Lyons T. W., Bekker A., Shen Y., Poulton S. W., Chu X. and Anbar A. D. (2008) Tracing the stepwise oxygenation of the Proterozoic ocean. *Nature* **452**(7186), 456–459.

Severmann S., Lyons T. W., Anbar A., McManus J. and Gordon G. (2008) Modern iron isotope perspective on the benthic iron shuttle and the redox evolution of ancient oceans. *Geology* **36**(6), 487–490.

Sinke A. J., Cornelese A. A., Cappenberg T. E. and Zehnder A. J. (1992) Seasonal variation in sulfate reduction and methanogenesis in peaty sediments of eutrophic Lake Loosdrecht, The Netherlands. *Biogeochemistry* **16**(1), 43–61.

Suits N. S. and Wilkin R. T. (1998) Pyrite formation in the water column and sediments of a meromictic lake. *Geology* **26**(12), 1099–1102.

Taillefert M. and Gaillard J. F. (2002) Reactive transport modeling of trace elements in the water column of a stratified lake: iron cycling and metal scavenging. *J. Hydrol.* **256**(1), 16–34.

Takahashi T., Broecker W., Li Y. H. and Thurber D. (1968) Chemical and isotopic balances for a meromictic lake. *Limnol. Oceanogr.* **13**(2), 272–292.

Tankere S. P. C., Muller F. L. L., Burton J. D., Statham P. J., Guieu C. and Martin J. M. (2001) Trace metal distributions in shelf waters of the Northwestern Black Sea. *Cont. Shelf Res.* **21**(13), 1501–1532.

Tebo B. M. (1991) Manganese (II) oxidation in the suboxic zone of the Black Sea. *Deep Sea Res. Part A: Oceanogr. Res. Pap.* **38**, S883–S905.

Tebo B. M., Bargar J. R., Clement B. G., Dick G. J., Murray K. J., Parker D., Verity R. and Webb S. M. (2004) Biogenic manganese oxides: properties and mechanisms of formation. *Annu. Rev. Earth Planet. Sci.* **32**, 287–328.

Thompson J. B., Ferris F. G. and Smith D. A. (1990) Geomicrobiology and sedimentology of the mixolimnion and chemocline in Fayetteville Green Lake, New York. *Palaios*, 52–75.

Thompson J. B., Schultze-Lam S., Beveridge T. J. and Des Marais D. J. (1997) Whiting events: biogenic origin due to the photosynthetic activity of cyanobacterial picoplankton. *Limnol. Oceanogr.* **42**(1), 133–141.

Tonolla, M., Demarta, A., and Peduzzi, R. (1998). The chemistry of Lake Cadagno. In *Lake Cadagno: a Meromictic Alpine Lake*. (eds. Peduzzi, R., Bachofen, R., and Tonalla, M.) *Documenta 1st. Ital. Idrobiol.*, 63: pp. 11–17.

Torgersen T., Hammond D. E., Clarke W. B. and Peng T. H. (1981) Fayetteville, Green Lake, New York: 3H–3He water mass ages and secondary chemical structure. *Limnol. Oceanogr.* **26**, 110–122.

Trefry J. H., Presley B. J., Keeney-Kennicutt W. L. and Trocine R. P. (1984) Distribution and chemistry of manganese, iron, and suspended particulates in Orca Basin. *Geo-Mar. Lett.* **4**(2), 125–130.

Turano V. S. and Rand M. C. (1967) Some chemical observations on Fayetteville Green Lake, New York. In *Some aspects of meromixis*. Syracuse University, Department of Civil Engineering, Syracuse, New York, pp. 152–187.

Van Cappellen P., Viollier E., Roychoudhury A., Clark L., Ingall E., Lowe K. and Dichristina T. (1998) Biogeochemical cycles of manganese and iron at the oxic–anoxic transition of a stratified marine basin (Orca Basin, Gulf of Mexico). *Environ. Sci. Technol.* **32**(19), 2931–2939.

Vorlicek T. P., Kahn M. D., Kasuya Y. and Helz G. R. (2004) Capture of molybdenum in pyrite-forming sediments: role of ligand-induced reduction by polysulfides. *Geochim. Cosmochim. Acta* **68**(3), 547–556.

Wang D., Aller R. C. and Sanudo-Wilhelmy S. A. (2011) Redox speciation and early diagenetic behavior of dissolved molybdenum in sulfidic muds. *Mar. Chem.* **125**(1), 101–107.

Xue H. B., Jansen S., Prasch A. and Sigg L. (2001) Nickel speciation and complexation kinetics in freshwater by ligand exchange and DPCSV. *Environ. Sci. Technol.* **35**(3), 539–546.

Yakushev E., Pakhomova S., Sørenson K. and Skei J. (2009) Importance of the different manganese species in the formation of water column redox zones: observations and modeling. *Mar. Chem.* **117**(1), 59–70.

Yao W. and Millero F. J. (1995) The chemistry of the anoxic waters in the Framvaren Fjord, Norway. *Aquat. Geochem.* **1**(1), 53–88.

Yebra-Biurrun M. C. and Castro-Romero J. M. (2011) Speciation of dissolved trace nickel in environmental waters by on-line sonodigestion-flow injection solid phase extraction coupled to flame atomic absorption spectrometry. *Am. J. Anal. Chem.* **2**(02), 116.

Yiğiterhan O., Murray J. W. and Tuğrul S. (2011) Trace metal composition of suspended particulate matter in the water column of the Black Sea. *Mar. Chem.* **126**(1), 207–228.

Zahalak M., Pratte B., Werth K. J. and Thiel T. (2004) Molybdate transport and its effect on nitrogen utilization in the cyanobacterium *Anabaena variabilis* ATCC 29413. *Mol. Microbiol.* **51**(2), 539–549.

Zerkle A. L., House C. H., Cox R. P. and Canfield D. E. (2006) Metal limitation of cyanobacterial N_2 fixation and implications for the Precambrian nitrogen cycle. *Geobiology* **4**(4), 285–297.

Zerkle A. L., Kamyshny, Jr, A., Kump L. R., Farquhar J., Oduro H. and Arthur M. A. (2010) Sulfur cycling in a stratified euxinic lake with moderately high sulfate: constraints from quadruple S isotopes. *Geochim. Cosmochim. Acta* **74**(17), 4953–4970.

Associate editor: David Johnston